Supporting information

Interplay of Diffusion and Crystallization in Sequentially Evaporated Lead Tin Perovskites

Lara M. van der Poll, Moisés Cámara Díaz, Reinder K. Boekhoff, Poojalakshmi Vageeswaran, Swapna Ganapathy, Lars J. Bannenberg, Dibyajyoti Ghosh, Arno H.M. Smets, and Tom J. Savenije

Table S1. Individual layer thicknesses used for the production of $FAPb_{0.5}Sn_{0.5}I_3$ perovskite films with different thicknesses (275nm, 500 nm, 750 nm) by sequential thermal evaporation using a single cycle (1c) or a double cycle (2c). Here, the tooling factor (TF) is defined as TF = (resulting film thickness) / (thickness measured on QCM).

Sample	**$PbSnI_4$ thickness (nm) (TF = 0.78)**	**FAI thickness (nm) (TF = 0.48)**
275 nm deposited in 1c	243.8	326.6
500 nm deposited in 1c	487.6	653.2
700 nm deposited in 1c	731.4	979.8
700 nm deposited in 2c	370 (c1) +370 (c2)	490 (c1) + 490 (c2)

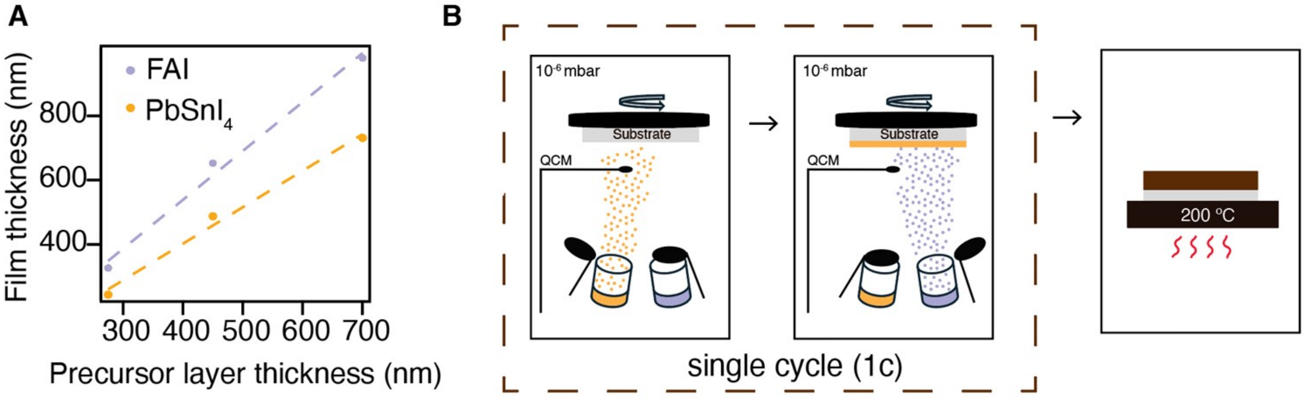

Figure S1. A. Final film thickness as a function of the layer thickness (as deposited on the QCM) for the individual FAI and $PbSnI_4$ precursors. **B.** Schematic representation of the sequential thermal evaporation process. The deposition steps included in a single cycle (1c) are indicated by a dashed line.

Table S2. Expected composition (atomic %) of $FAPb_{0.5}Sn_{0.5}I_3$.

	I	**N**	**C**	**Pb**	**Sn**
Theoretical	42.9%	28.6%	14.3%	7.1%	7.1%

Table S3. Pb:Sn:I ratio of each combination of sample thickness and number of deposition cycles employed. This data was extracted from XPS measurements.

	Pb	**Sn**	**I**
500 nm 1c	0.179	0.151	0.669
500 nm 2c	0.188	0.148	0.664
700 nm 1c	0.189	0.163	0.648
700 nm 2c	0.184	0.170	0.647

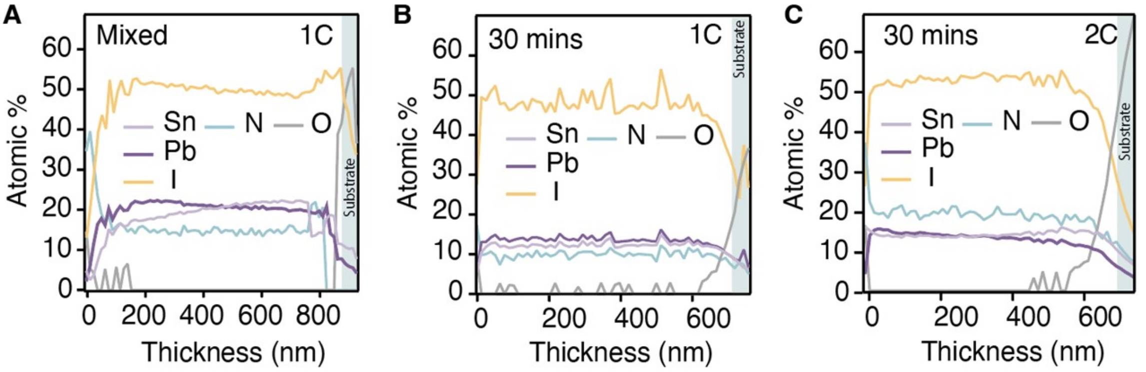

Figure S2. Compositional XPS depth profiles of different FA$Pb_{0.5}Sn_{0.5}I_3$ samples made in a single cycle of sequential thermal evaporation. **A.** Unannealed film measured at least 12 hours after the deposition to allow the precursors to mix. **B.** Film annealed for 30 minutes at 200 °C. **C.** Compositional XPS profile of a sample deposited in a double cycle (2c) and annealed for 30 minutes at 200 °C.

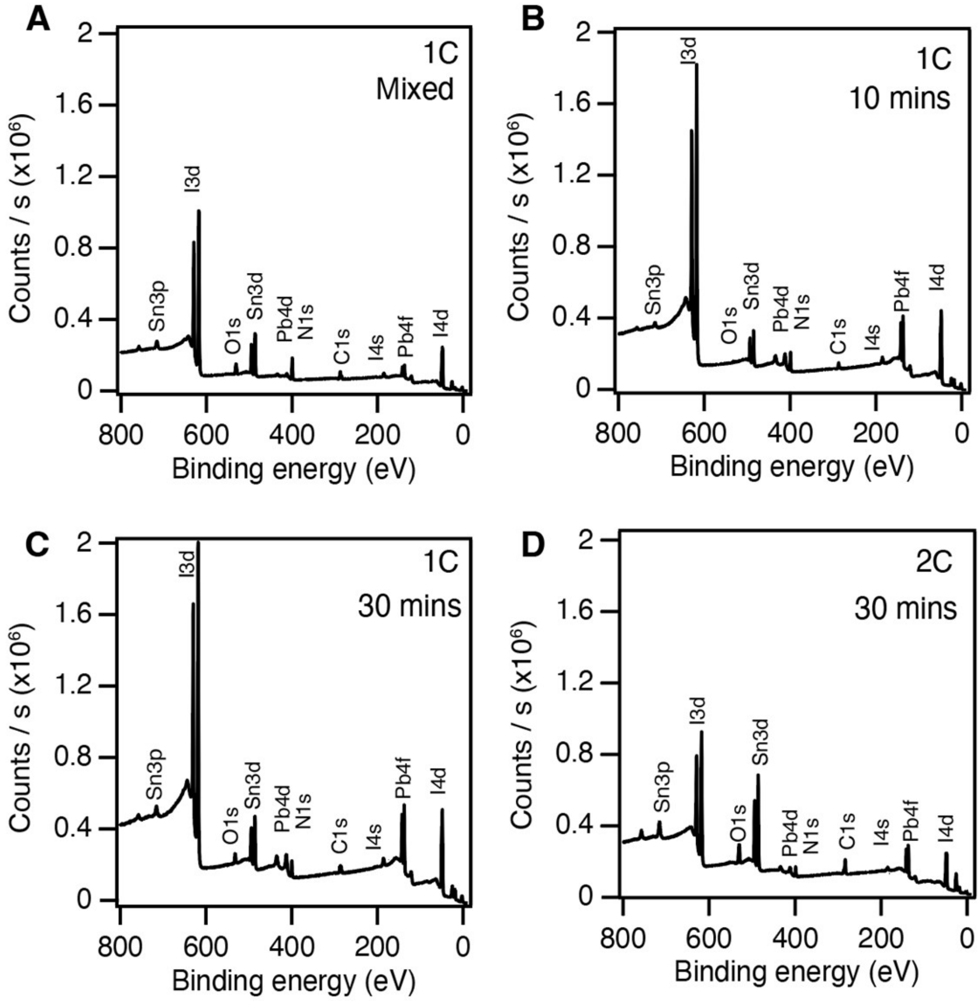

Figure S3. XPS survey scans of FA$Pb_{0.5}Sn_{0.5}I_3$ samples deposited in a single cycle (1c) of sTE and **A.** left overnight in the glovebox to mix, and annealed for **B.** 10 and **C.** 30 minutes at 200 °C. Survey scan of PVK sample deposited in a double cycle (2c) of sTE and annealed for 30 minutes at 200 °C.

Table S4. Device parameters of the champion devices, including 500 nm and 700 nm thick absorber layers.

	J_{sc} (mA/cm^2)	V_{oc} (V)	FF (%)	R_{shunt} (Ω cm^2)	R_{series} (Ω cm^2)	V_{mp} (V)	J_{mp} (mA/cm^2)	PCE (%)
After deposition	30.53	0.6226	64.15	290.6	2.607	0.483	25.25	10.16
From mixed	30.89	0.6116	65.71	434.8	2.553	0.472	26.32	10.35
700 nm PVK	35.16	0.5526	60.53	489.7	2.333	0.409	28.74	9.802

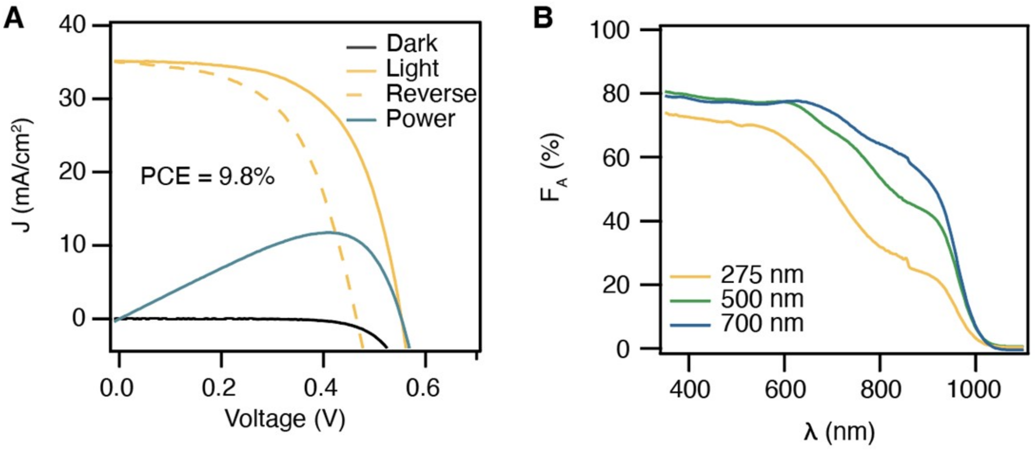

Figure S4. A. Champion JV curve of a device with architecture ITO/PEDOT:PSS/$FAPb_{0.5}Sn_{0.5}I_3$ (700 nm)/C60/BCP/Ag. The reverse scan and the power output are also included. **B.** Absorbance data for $FAPb_{0.5}Sn_{0.5}I_3$ PVK films of different thicknesses (275, 500, and 750 nm).

Table S5. Quasi-Fermi level splittings (QFLS) of bare PVK film and stacks, including the ETL (C60) and HTL (PEDOT:PSS), annealed immediately after the deposition or left to mix overnight before annealing**.**

Sample	QFLS after deposition	QFLS from mixed
PVK	0.82 eV	0.81 eV
PVK/C60	0.87 eV	0.83 eV
PEDOT:PSS/PVK	0.71 eV	0.73 eV
PEDOT:PSS/PVK/C60	0.69 eV	0.68 eV

1C

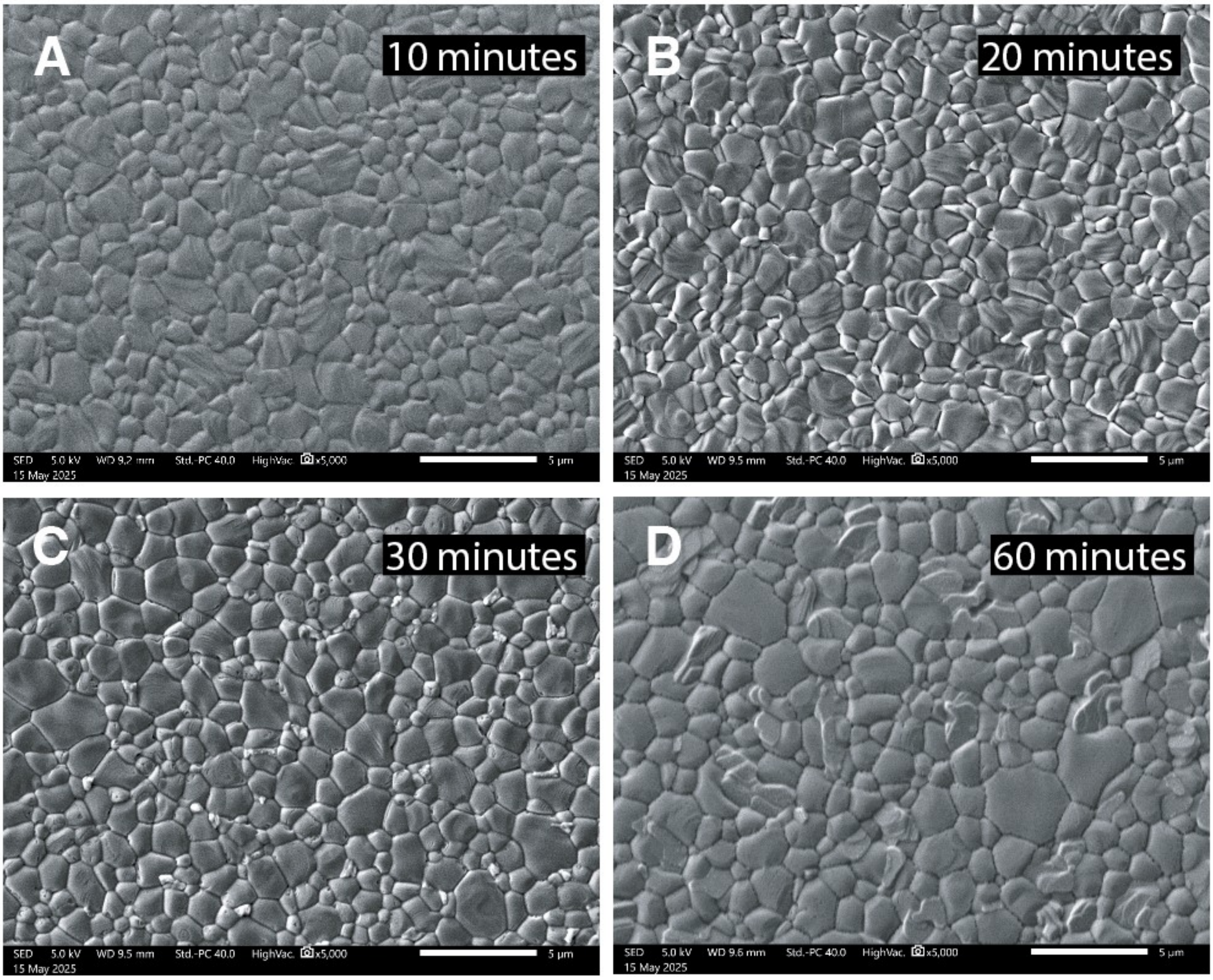

Figure S5. Top-view SEM images of (1c) $FAPb_{0.5}Sn_{0.5}I_3$ perovskite films annealed at 200 °C for **A.** 10, **B.** 20, **C.** 30, and **D.** 60 minutes. All micrographs were taken at a x5k magnification. The scale bars indicate 5 µm.

2C

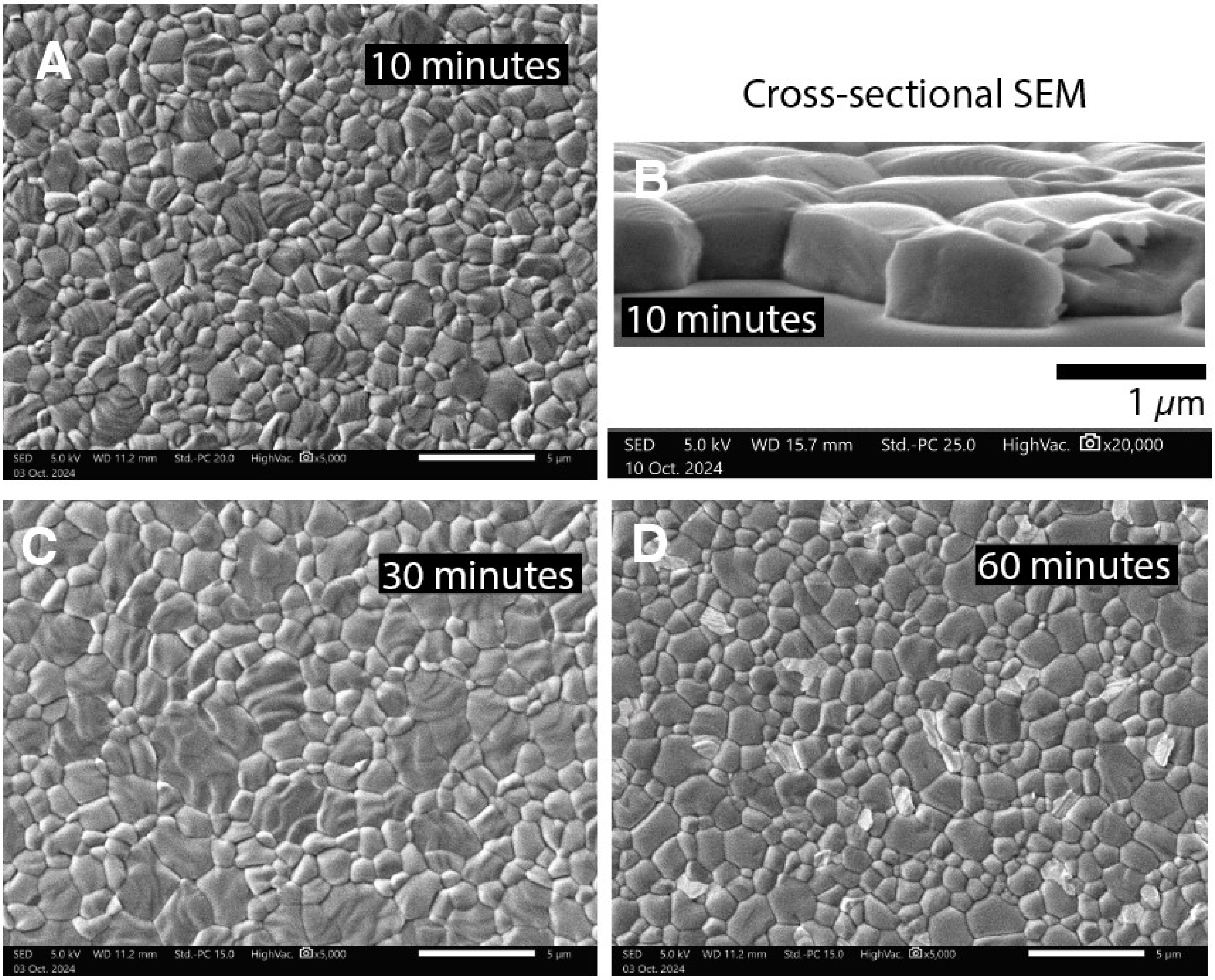

Figure S6. SEM images of (1c) FAPb$_{0.5}$Sn$_{0.5}$I$_3$ perovskite films annealed at 200 °C for **A.** 10 (top-view), **B. 1**0 (side-view), **C.** 30 (top-view), and **D.** 60 minutes (top-view).

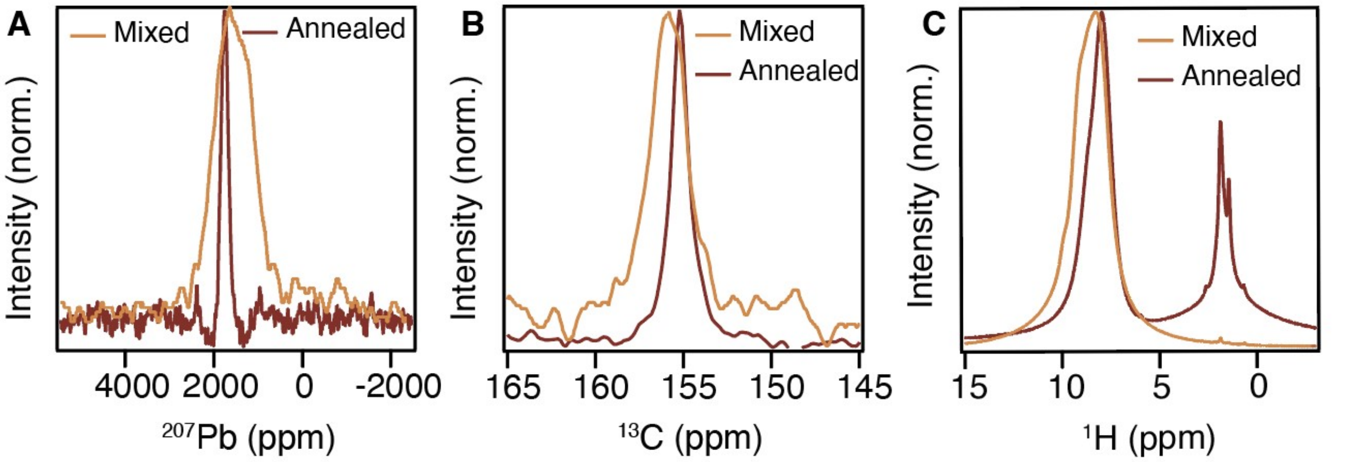

Figure S7. A. Normalized MAS ^{207}Pb solid-state NMR results for the mixed material and the annealed PVK film. **B.** Normalized MAS ^{13}C solid-state NMR results for the mixed material and the annealed PVK film. **C.** Normalized MAS ^{1}H solid-state NMR results for the mixed material and the annealed PVK film.

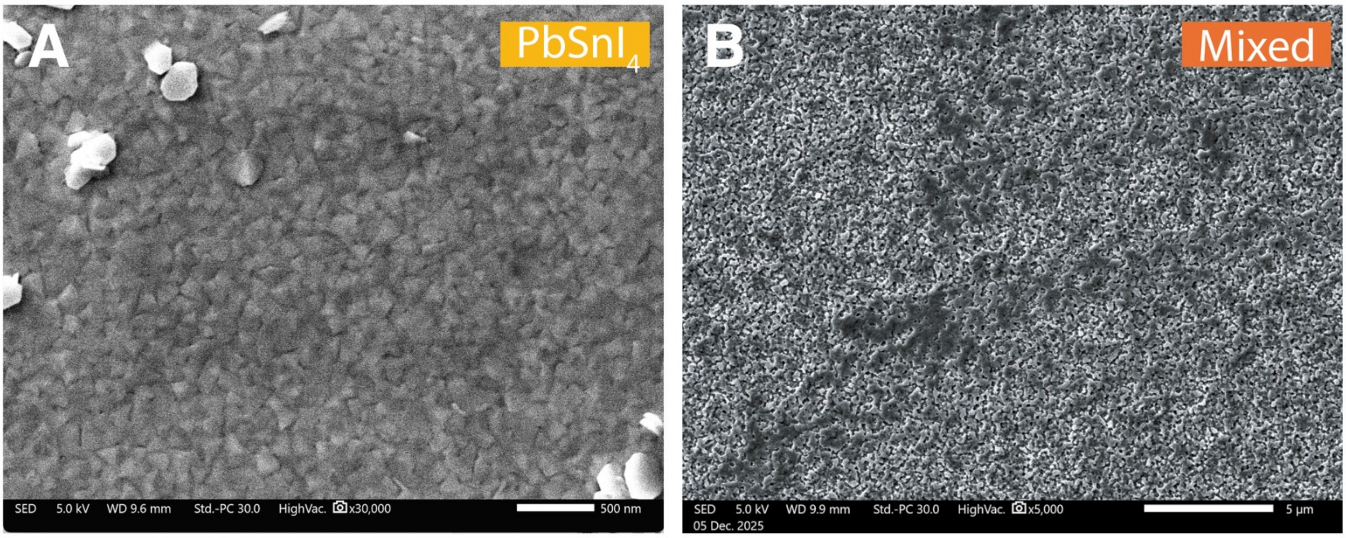

Figure S8. Top-view SEM image of **A.** evaporated PbSnI$_4$ film, scale bar indicates 500 nm, and **B.** PVK film that was left in the glovebox overnight to allow precursor diffusion. The scale bar indicates 5 µm.

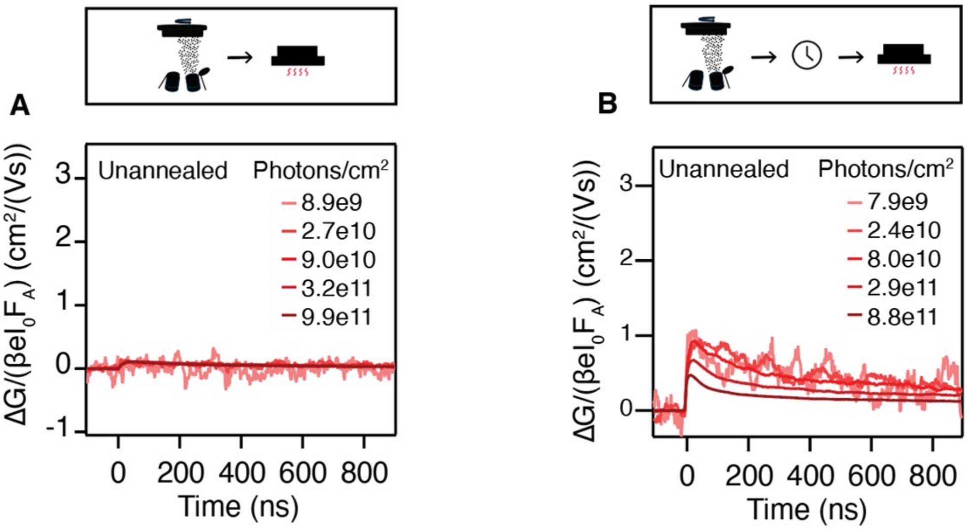

Figure S9. Transient photoconductance traces, normalized by a geometric factor (β), the electronic charge constant (e), the incident light intensity (I_0), and F_A, to express the data as a yield-mobility product for unannealed perovskite films immediately after deposition and left to mix overnight.

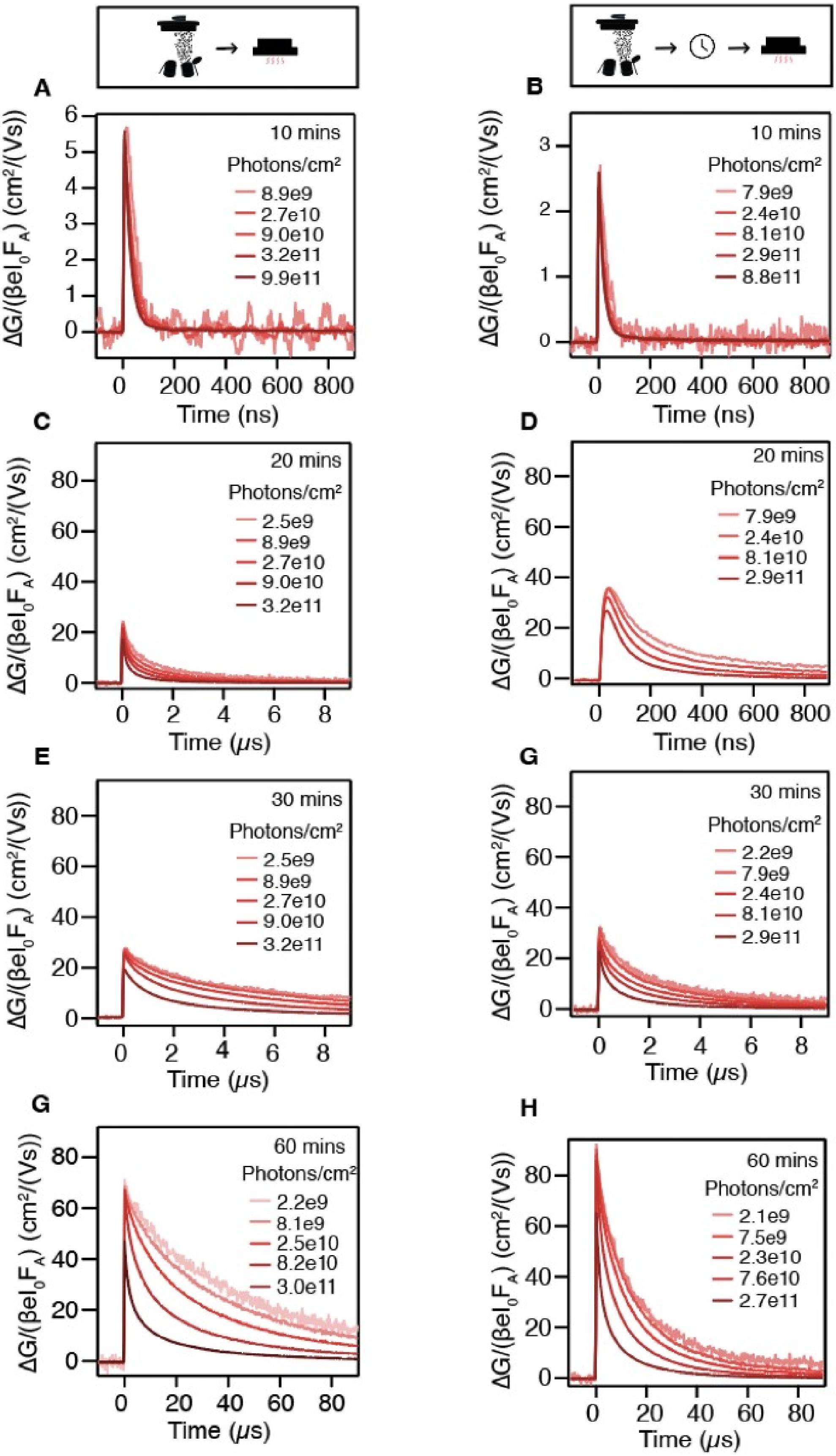

Figure S10. Transient photoconductance traces, normalized by a geometric factor (β), the electronic charge constant (e), the incident light intensity (I_0), and F_A, to express the data as a yield-mobility product for perovskite films annealed at 200 °C for 10, 20, 30, and 60 minutes and annealed immediately after deposition and left to mix overnight before annealing.

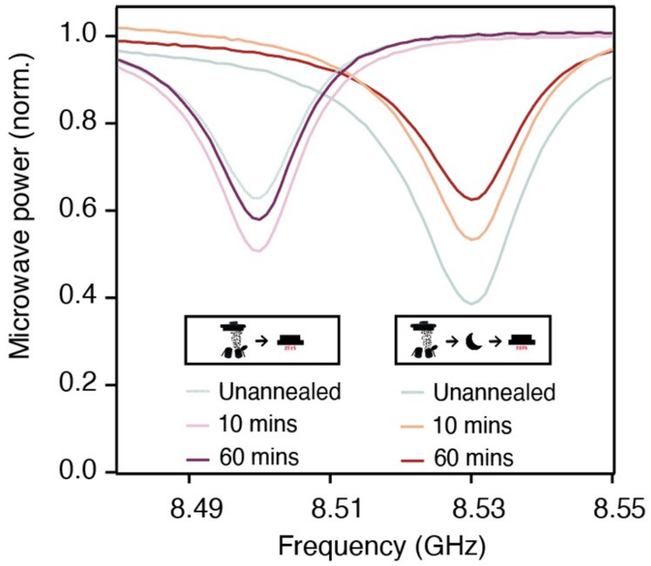

Figure S11. Steady-state microwave conductivity (SSMC) data reported as the normalized microwave power as a function of resonance frequency for the samples annealed directly after the deposition (left) and samples annealed after being left to mix overnight (right).

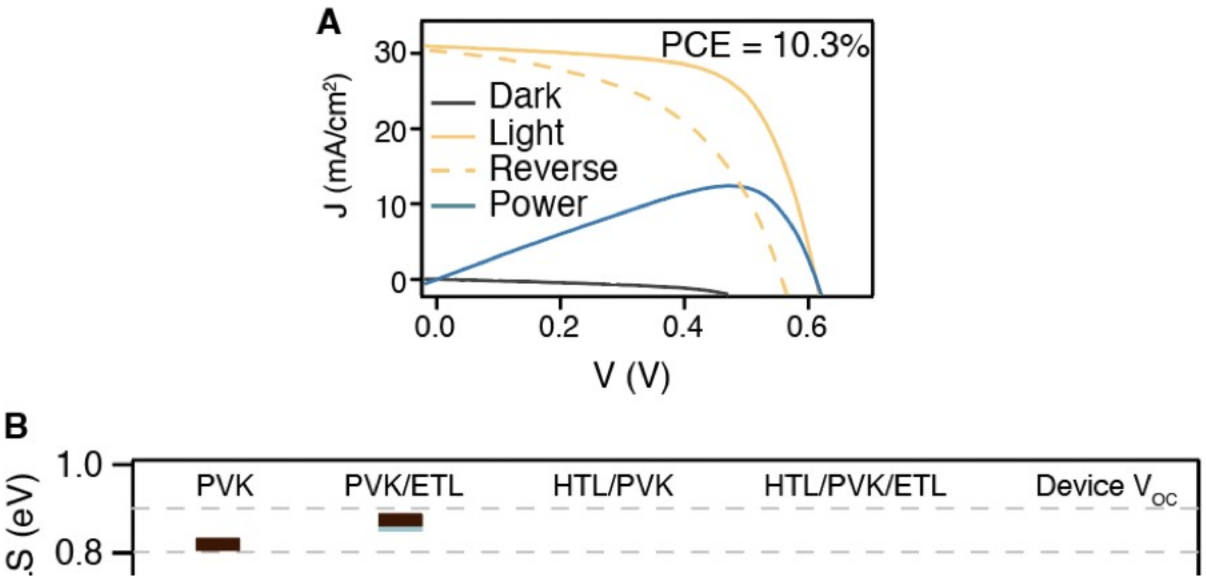

Figure S12 A. Champion JV curve of a device with architecture ITO/PEDOT:PSS/FAPb$_{0.5}$Sn$_{0.5}$I$_3$ (500 nm)/C60/BCP/Ag. In this device, the PVK films (processed on top of PEDOT:PSS) was left to mix overnight before annealing at 200 °C for 30 minutes. The reverse scan and the power output are also included. **B.** Quasi-Fermi level splitting data for the bare PVK layers as well as the partial stacks with the HTL (PEDOT:PSS) and the ETL (C60). Plotted together with the device open-circuit voltage (V$_{OC}$).

Photoconductance measurements

Microwave conductivity measurements were used to study the dark conductivity and the photoconductance of the perovskite films. In this technique, the reduction in microwave power is directly related to a change in conductivity. By use of **equation S1**, where the microwave power (ΔP) is normalized using the initial microwave power (P) and set equal to the product of the sensitivity factor (K) and the change in photoconductance induced (ΔG):

$$\frac{\Delta P}{P} = - K\Delta G \qquad \text{(S1)}$$

The sensitivity of the measurement is greatly enhanced due to the use of a resonant cavity as a measurement cell. The cavity is designed in such a way that allows the sample to be placed at the maximum of the standing wave that forms at the resonance frequency. This ensures maximum overlap between the microwave and the sample.

Dark (DMC): To determine the dark conductivity and the resonance frequency of the cavity, DMC measurements are used. Here, the microwave frequency is swept between 8.5 – 12.1 GHz while the reflected microwave power is measured. Usually, the DMC data is reported in a normalized fashion ($\frac{\Delta P}{P}$), with P the initial microwave power (~100 mW). A dip in the DMC data only occurs at the resonant frequency, while the depth of the dip is related to the dark conductivity.

Time-Resolved (TRMC): To record the transient photoconductance signals, pulsed laser illumination is used at a repetition rate of 10 Hz from a Nd:YAG laser with a pulse width of 3-5 ns at FWHM. All measurements were performed using a wavelength of 800 nm. The light intensity was adapted using a set of neutral density filters. The photogenerated carriers interact with the standing microwave, which results in a change of the microwave power over time ($\frac{\Delta P(t)}{P}$). Using a predetermined sensitivity factor K, $\frac{\Delta P(t)}{P}$) can be related to a change in photoconductance ($\Delta G(t)$), using **equation S2**.

$$\frac{\Delta P(t)}{P} = - K\Delta G(t) \qquad \text{(S2)}$$

The TRMC signal is usually normalized by the electric charge constant (e), the fraction of absorbed light (F_A), the incoming light intensity (I_0), and a geometric factor (β), which takes into account the inner dimensions of the cavity. This way, the signal can be expressed as the yield-mobility product, as shown in **equation S3**, where φ is the charge carriers yield, which is set to unity. Also, μ_e and μ_h are the electron and hole mobility, respectively.

$$\varphi(\mu_e + \mu_h) = \frac{\Delta G}{\beta e F_A I_0} \qquad \text{(S3)}$$

LED-modulated microwave conductivity measurements (LMMC): To determine the quasi-Fermi level splitting (QFLS), a monochromatic LED (λ = 522 nm) is used to photogenerate carriers. The light is modulated with a frequency of 1 Hz. The microwave source is set to the resonance frequency previously determined by SSMC. The change in voltage (ΔV) is recorded by use of a lock-in amplifier and related to the change in microwave power using **equation S4**. Here, the number N is extracted from a look-up table and is a function of the resonant microwave frequency and the cell voltage in the dark (V_{cell}).

$$N\frac{\Delta V}{V_{cell}} = \frac{\Delta P}{P} \qquad \text{(S4)}$$

The change in microwave power is then used to determine the change in conductivity ($\Delta\sigma$), using **equation S5** and the sample thickness L.

$$\frac{\Delta P}{P} = - K\beta L\Delta\sigma \qquad \text{(S5)}$$

Given that each photon results in the equal generation of excess holes (Δn_h) and electrons (Δn_e), the total excess carrier concentration (Δn) is determined using **equation S6**.

$$\Delta\sigma = e(\mu_e \Delta n_e + \mu_h \Delta n_h) = e\Delta n(\mu_e + \mu_h) \qquad \text{(S6)}$$

Finally, from SSMC measurements, it can be determined that the dark carrier concentrations (n_0,p_0) are smaller than the generated carrier densities and thus can be disregarded. Now, the QFLS is calculated using **equation S7**.

Here, $\frac{k_BT}{q}$ is the thermal voltage and n_i the intrinsic carrier density (10^8 photons/cm^2).

$$QFLS = \frac{k_BT}{q} ln(\frac{(n_0 + \Delta n_e)(p_0 + \Delta n_h)}{n_i^2}) = \frac{k_BT}{q} ln(\frac{\Delta n^2}{n_i^2}) \qquad (S7)$$